Sensors & Diagnostics

PAPER

View Article Online
View Journal | View Issue

Cite this: *Sens. Diagn.*, 2023, **2**, 665

A benzimidazole-derived fluorescent chemosensor for Cu(II)-selective turn-off and Zn(II)-selective ratiometric turn-on detection in aqueous solutions†

Wan-Yu Zhu,[a] Kai Liu *[a] and Xuan Zhang *[ab]

Received 14th January 2023,
Accepted 6th March 2023

DOI: 10.1039/d3sd00020f

rsc.li/sensors

A 2,6-dibenzoimidazolyl-4-methoxyphenol conjugate (BBMP) was designed and synthesized to develop a novel fluorescent chemosensor for Cu^{2+} and Zn^{2+}. The as-fabricated BBMP showed an excited-state intramolecular proton-transfer (ESIPT) fluorescence emission at 542 nm that was selectively and efficiently quenched by Cu^{2+} in a Tris-HCl solution (70% THF, pH = 7.4) due to the inhibition of ESIPT upon binding to metal ions. In contrast, the addition of Zn^{2+} not only resulted in a substantial decline in the original ESIPT fluorescence of BBMP but was also accompanied by the appearance of a new blue fluorescence emission at 462 nm. This indicated the potential for the present BBMP as a novel fluorescent probe for Cu^{2+} (turn-off) and Zn^{2+} (ratiometric turn-on) detection in aqueous solutions. The linear range and detection limit were found to be 0–5 μM and 0.16 μM for Cu^{2+}, as well as 0–10 μM and 0.1 μM for Zn^{2+}, respectively. A 2 : 1/1 : 1 coordination mode between BBMP and Cu^{2+}/Zn^{2+} was confirmed by Job plots and mass analysis. Potential practical applications were also demonstrated by the analysis of real water samples and living cell imaging.

1. Introduction

The design and development of organic small-molecule fluorescent chemosensors for the detection of various metal ions has attracted extensive attention.[1–4] Zn^{2+} and Cu^{2+} are known to be important trace elements that are involved in many physiological processes.[5,6] However, it has also been noted that an imbalance of Zn^{2+} and Cu^{2+} concentrations can lead to various diseases, such as metabolic disorders, Parkinson's disease, and coronary heart disease.[7–10] Hence, it would be of great significance to develop a highly selective and sensitive fluorescent chemosensor to quantitatively detect Cu^{2+} and Zn^{2+} in biological and environmental fields. In this regard, a number of fluorescent sensors for Cu^{2+} and Zn^{2+} detection have been designed based on various coordination scaffolds.[9–27] For example, a naphthalene Schiff-base system was designed as a fluorescent sensor for Cu^{2+} and Zn^{2+}, where the fluorescence of the sensor was quenched by Cu^{2+}or enhanced by Zn^{2+} over other metal cations in DMSO, respectively.[11] Kim *et al.* reported a phenanthrene-based multifunctional chemosensor that showed a slightly enhanced and blue-shifted (45 nm) fluorescence emission in the presence of Zn^{2+}, whereas Cu^{2+} caused a serious quenching of the original fluorescence.[18] Recently, a dual-functional Schiff-base fluorescent sensor containing the coumarin fluorophore was developed for Zn^{2+} and Cu^{2+} detection, in which Zn^{2+} induced a red-shift (46 nm) of the emission wavelength, allowing it to be used for the construction of a molecular logic gate with metal ion inputs and fluorescence signal outputs.[22] Even the dual recognition of different Cu^{2+} and Zn^{2+} ions by a single sensor has been achieved, but most of their fluorescence emission showed no distinct or just a slight shift from the original one over binding events. It is practically undesirable for a dual-functional fluorescent chemosensor to be used for two different metal ions due to the discrimination being more difficult to as ascertain from a fluorescence intensity change than from a color change. Moreover, it has been considered that the fluorescence intensity is usually dependent on the measurement conditions, such as the concentration, excitation light intensity, and instrument efficiency, and that a ratiometric fluorescent sensor could overcome such shortcomings.[3,28,29] Therefore, a dual-functional fluorescent sensor for Cu^{2+} and Zn^{2+} that could exhibit a large emission

[a] *Key Laboratory of Science and Technology of Eco-Textiles, Ministry of Education, College of Chemistry and Chemical Engineering, Donghua University, Shanghai 201620, China. E-mail: kailiu@dhu.edu.cn, xzhang@dhu.edu.cn*
[b] *National Innovation Center of Advanced Dyeing & Finishing Technology, Tai'an, Shandong 271000, China*

† Electronic supplementary information (ESI) available. See DOI: https://doi.org/10.1039/d3sd00020f

wavelength shift from the original one upon binding with metal ions would be promising for a ratiometric sensor, but would be challenging to achieve.[30]

Recently, benzimidazole-containing fluorescent sensors have attracted much interest due to their nice coordination ability toward metal ions.[31–36] Anbu *et al.* reported a benzimidazole-based Schiff-base-type fluorescent sensor that could differentially detect Cu^{2+} and Zn^{2+} through a fluorescence on–off and enhancement manner, respectively.[36] However, in the case of Zn^{2+} detection, the fluorescence emission was only blue-shifted by 10 nm. In this work, we designed and developed the novel benzimidazole-derived fluorescent sensor BBMP (Scheme 1) for Cu^{2+} and Zn^{2+}. The present BBMP exhibited an excited-state intramolecular proton-transfer (ESIPT) emission at 542 nm and fluorescence quenching upon binding to Cu^{2+} and Zn^{2+} due to the inhibition of ESIPT. Notably, the BBMP also showed an 82 nm blue-shifted fluorescence emission upon binding to Zn^{2+}, allowing ratiometric detection. Thus a benzimidazole-derived fluorescent sensor was developed for Cu^{2+}-selective turn-off and Zn^{2+}-selective ratiometric turn-on detection in aqueous solution. Furthermore, this was successfully used for Cu^{2+} and Zn^{2+} detection in real water samples and for fluorescence imaging in living cells, respectively.

2. Experimental

2.1. Materials and methods

4-Nethoxyphenol, hexamethylenetetramine, *o*-phenylenediamine, trifluoroacetic, hydrochloride acid, and all organic solvents were analytical grade and purchased from Sinopharm Chemical Reagents Co. (Shanghai, China). The solutions of metal cations were prepared by dissolving the corresponding perchlorates (Mg^{2+}, Hg^{2+}), chlorides (Ca^{2+}, Al^{3+}, Mn^{2+}, Co^{2+}, Pd^{2+}), sulfates (Fe^{2+}, Cu^{2+}), or nitrates (Fe^{3+}, Ni^{2+}, Zn^{2+}, Ag^{+}, Cd^{2+}, Pb^{2+}) salts with deionized water (10 mM). The stock solution of the BBMP sensor (1 mM) was dissolved in DMSO and the working solution was obtained by dilution with Tris-HCl buffer solution (10 mM, pH 7.4). The prepared solution was used for spectral testing and cellular imaging.

An Edinburgh FS5 spectrofluorometer was employed to measure the fluorescence spectra at room temperature (the slit width was set to 5 nm for both excitation and emission). Absolute fluorescence quantum yield measurements were carried out on an Edinburgh FS5 spectrofluorometer equipped with an integrating sphere (EI-FS5-SC-30). The UV-vis absorption spectra were collected on a Shimadzu UV-1800 spectrophotometer. The ^{1}H and ^{13}C NMR spectra were recorded on a Bruker AVANCE III 400 MHz spectrometer with TMS as the internal standard. The high-resolution mass spectra were obtained on Micro TOFII 10257, Agilent 7250, and JEOL-JMS-T100LP AccuTOF mass spectrometers, respectively.

For analysis of real water samples, lake water and drinking water samples were collected from Songjiang Campus of Donghua University and a water dispenser, respectively. Zinc gluconate oral liquid (Harbin Pharm Group Sanjing Pharmaceutical Co. Ltd, China) was purchased from a local medical store. Fluorescence imaging in living HeLa cells was observed by an Axio Vert, A1 Carl Zeiss fluorescence microscopy system (Jena, Germany).

2.2. Synthesis of BBMP

The BBMP sensor was synthesized by a concise two-step process, as summarized in Scheme 1. First, 2,6-diformyl-4-methoxyphenol was synthesized according to our previously works.[37–39] Specifically, under a N_2 atmosphere, 4-methoxyphenol (15 mmol) and hexamethylenetetramine (45 mmol) were dissolved in trifluoroacetic acid (25 mL) and refluxed at 110 °C for 72 h. The mixture was cooled to 90 °C and 1 M HCl solution was added and stirring was continued for 24 h. The mixture was filtered and the filtrate was extracted with dichloromethane (25 mL × 3). Then the filtered solid and the extract were combined and washed with water until neutral pH. The organic phase was dried over anhydrous Na_2SO_4 for half an hour and concentrated under reduced pressure evaporation. The crude product was further purified by column chromatography (silica gel, ethyl acetate : petroleum ether = 1 : 10). Finally, a yellow flocculent solid was obtained. Yield, 30%. ^{1}H NMR (400 MHz, chloroform-d), δ (ppm): 11.13 (s, 1H), 10.22 (s, 2H), 7.51 (s, 2H), 3.86 (s, 3H).

Subsequently, under a N_2 atmosphere, 2,6-diformyl-4-methoxyphenol (1 mmol) and *o*-phenylenediamine (2.4 mmol) were dissolved in dichloromethane (15 mL) and refluxed for 63 h. After the reaction was completed, the mixture was cooled to room temperature, and the crude

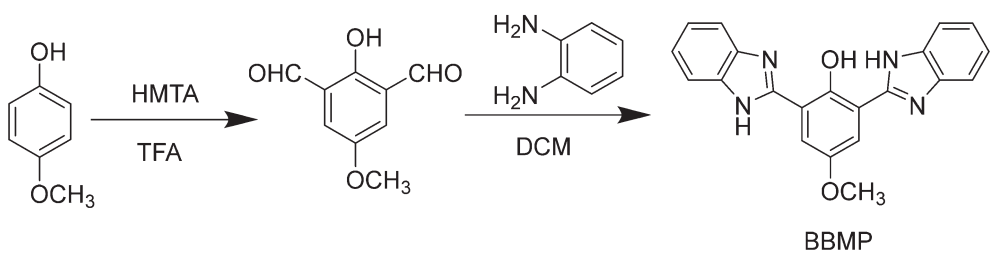

Scheme 1 Synthesis of BBMP.

product was obtained by filtration, and washed with dichloromethane three times to obtain the target BBMP as an orange solid. Yield, 16.7%. ^{1}H NMR (400 MHz, DMSO-d_6), δ (ppm): 13.50 (s, 3H), 7.95 (s, 2H), 7.71 (dd, J = 6.0, 3.0 Hz, 4H), 7.29 (dd, J = 6.0, 3.0 Hz, 4H), 3.92 (s, 3H); ^{13}C NMR (101 MHz, DMSO-d_6), δ (ppm): 152.26, 150.86, 150.37, 138.01, 123.20, 116.38, 115.57, 115.08, 56.37. MS: m/z calcd for $C_{21}H_{16}N_4O_2$ 357.1347 $(M + H)^+$; found 357.1352 $(M + H)^+$.

3. Results and discussion

3.1. Photophysical properties of BBMP

The absorption and fluorescence spectra of BBMP were first studied in various solvents (Fig. 1). It could be seen that BBMP showed a yellowish-green fluorescence emission at 548 nm and two absorption peaks around 300 nm as well as 375 nm in the weak polar solvents DEE, $CHCl_3$, and THF, respectively. Notably, the fluorescence emission of BBMP at 548 nm was slightly blue-shifted several nanometers in the strong polar solvents DMSO, DMF, and MeOH, accompanied by the appearance of weak fluorescence around 470 nm, respectively (Fig. 1a). Meanwhile, a new and broad absorption peak was discernable at 400–500 nm in these polar solvents (Fig. 1b). The large Stokes shift (*ca.* 8400 cm^{-1}) and similar molecular structure feature to 2-(2-hydroxyphenyl) benzimidazole most probably indicated an ESIPT emission nature.[40] Therefore, the solvent-dependent photophysical properties could be tentatively rationalized according to a subtle solvent effect on the intramolecular hydrogen-bond interaction between the imidazole N atom and phenolic OH in BBMP. The weak polar solvents DEE, $CHCl_3$, and THF had little effect on the intramolecular hydrogen bonds in BBMP, and thus normal ESIPT emission was observed at 548 nm, without disturbance to the absorption spectra. In contrast, the strong polar solvents DMSO, DMF, and MeOH, could cause competition between the intermolecular and intramolecular hydrogen-bond interactions, as confirmed by the observation of a substantial change in the absorption and fluorescence spectra in these polar solvents. The more prominent change in DMF and MeOH could be related to their basic and protic nature, respectively. ESIPT emission only underwent a slight disturbance in the polar solvents, indicating that strong intramolecular hydrogen-bond interactions existed in BBMP. Interestingly, when NaOH was introduced into the THF solution of BBMP, a largely blue-shifted fluorescence emission at 490 nm and a red-shifted absorption band at 407 nm were observed (Fig. 1). It could be ascribed to the ESIPT being completely inhibited due to the anionic BBMP formed by the deprotonation in the presence of a strong base, as has previously been observed in 2-(2-hydroxyphenyl)benzothiazole derivatives.[41] In addition, the absolute fluorescence quantum yields of BBMP were measured to be in the range of 0.6–0.9 in various solvents (Table S1†).

3.2. Selectivity toward Zn^{2+} and Cu^{2+} detection

Then the selectivity of BBMP toward various metal ions was investigated in aqueous solution (pH 7.4 Tris-HCl buffer containing 70% THF) as shown in Fig. 2. Without metal ions, the BBMP sensor showed a strong yellowish-green ESIPT fluorescence at 542 nm under excitation at 370 nm. Significant fluorescence quenching was observed in the presence of Cu^{2+}, whereas Zn^{2+} selectively induced only a moderate quenching of the original ESIPT emission accompanied by the appearance of new blue fluorescence at 462 nm (Fig. 2a). In contrast, the fluorescence of BBMP showed almost no obvious change in the presence of other metal ions (Ca^{2+}, Mg^{2+}, Al^{3+}, Mn^{2+}, Fe^{3+}, Fe^{2+}, Ni^{2+}, Pd^{2+}, Ag^+, Cd^{2+}, Hg^{2+}, Pb^{2+}), except for Co^{2+}, which caused a slight quenching effect. This demonstrated that the present BBMP could serve as a novel fluorescent sensor for Cu(II)-selective turn-off and Zn(II)-selective ratiometric turn-on detection in aqueous solution. Fig. 2b shows the absorption spectra of BBMP in the absence and presence of various metal ions. Obviously red-shifted absorption was observed upon the addition of Cu^{2+}, Zn^{2+}, and Co^{2+} respectively, suggesting that

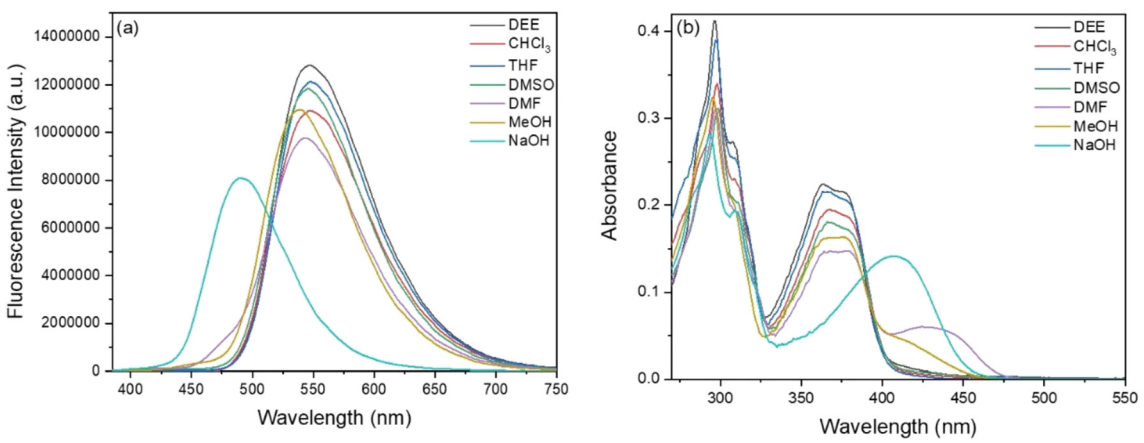

Fig. 1 Fluorescence (a) and absorption (b) spectra of BBMP (10 μM) in various solvents. The excitation wavelength was 370 nm.

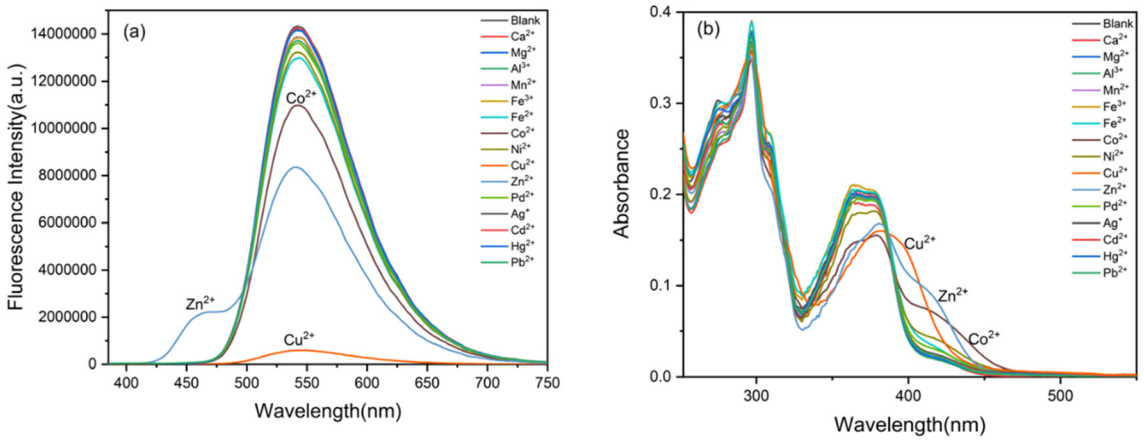

Fig. 2 Fluorescence (a) and absorption (b) spectra of BBMP (10 μM) upon the addition of 1 equiv. of various metal ions in Tris-HCl aqueous solution (10 mM, pH 7.4, containing 70% THF). The excitation wavelength was 370 nm.

BBMP could substantially coordinate with these metal ions. Combined with the photophysical properties of BBMP in various solvents (Fig. 1), it could tentatively be concluded that the ESIPT emission was inhibited upon binding to the metal ions.

To further examine the potential interference of others metal ions toward Cu^{2+} and Zn^{2+} detection, competition experiments were also conducted by measuring the fluorescence intensity at 542 nm and the intensity ratio at 462/541 nm. Fig. 3 shows that no significant interference was observed in the turn-off detection of Cu^{2+} and ratiometric turn-on detection of Zn^{2+}, respectively. Thus, the present BBMP sensor could selectively and differentially detect Cu^{2+} and Zn^{2+} in aqueous solution.

3.3. Response time and effect of the pH

To obtain the optimal detection conditions, the response time and effect of the pH were investigated. As shown in Fig. 4a, upon the addition of 1 equiv. Cu^{2+}, the fluorescence of BBMP (10 μM) at 542 nm rapidly declined but became stable within 2 min. In the case of Zn^{2+}, the fluorescence intensity ratio of 465/541 nm increased to the maximum within 3 min (Fig. 4b). This indicated that the response of BBMP toward Cu^{2+} and Zn^{2+} was fast, and all the solution measurements were therefore performed after standing for 3 min.

Subsequently, the fluorescence of BBMP in the absence and presence of 1 equiv. Cu^{2+} and Zn^{2+} was tested in the pH range of 2–11, respectively. It was found that the yellowish-green fluorescence of BBMP almost remained constant at pH <9, while the intensity at 542 nm slightly declined between pH 9–10, and a blue fluorescence emission appeared at 489 nm at pH >10 (Fig. 5a and S1a†). This could be attributed to deprotonation of the phenolic OH in BBMP and as anionic BBMP was produced at pH >10. In the presence of Cu^{2+}, the fluorescence of BBMP was drastically quenched at pH <10, and also a blue fluorescence at 489 nm was observed at pH >10 originating from the anionic BBMP (Fig. 5a and S1b†). Notably, upon the addition of 1 equiv. Zn^{2+}, the yellowish-green fluorescence of BBMP was slightly changed at pH <6 and

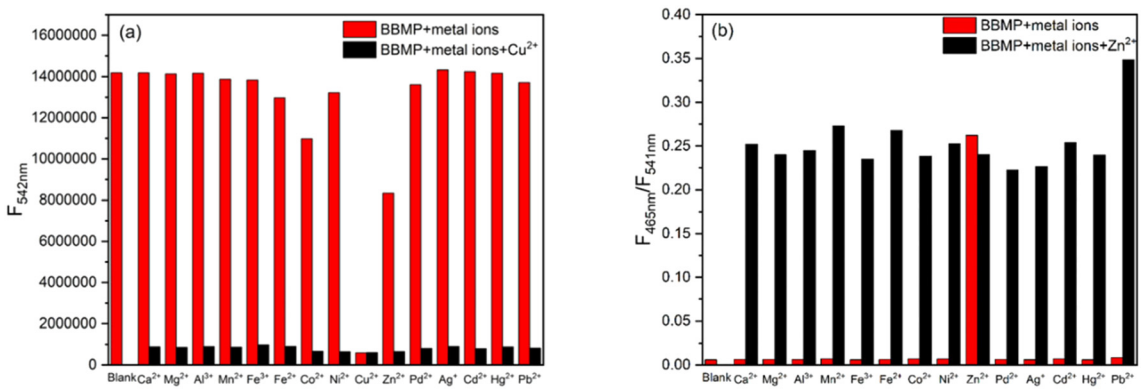

Fig. 3 Competition experiments for Cu^{2+} (a) and Zn^{2+} (b) in aqueous Tris-HCl solution (10 mM, pH 7.4, 70% THF). The excitation wavelength was 370 nm.

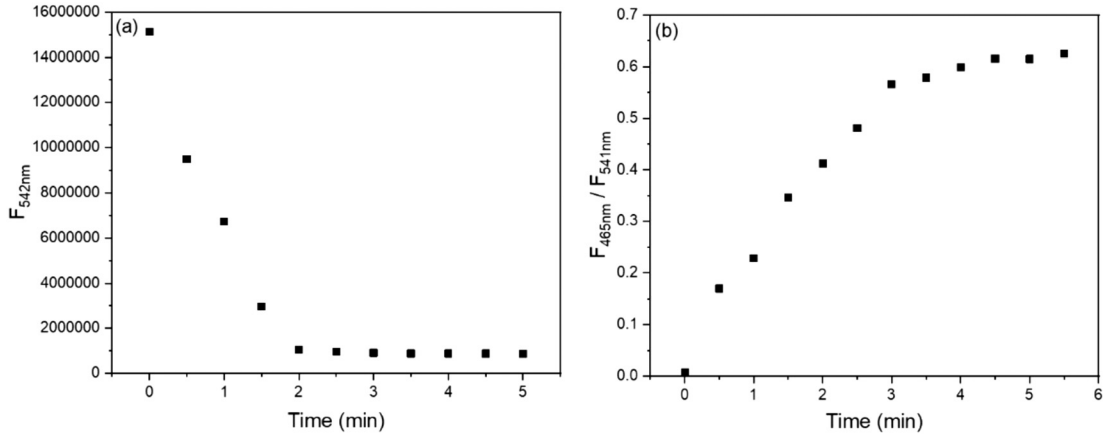

Fig. 4 Change in the fluorescence intensity of BBMP (10 μM) with time upon the addition of 1 equiv. Cu^{2+} (a) and Zn^{2+} (b) in aqueous Tris-HCl solution (10 mM, pH 7.4, 70% THF), respectively. The excitation wavelength was 370 nm.

moderate quenching was observed between pH 7–10, accompanied by the appearance of new blue fluorescence emission at 465 nm (Fig. 5b and S1c†). This allowed the ratiometric fluorescence detection of Zn^{2+}. Similarly, blue fluorescence at 489 nm from the anionic BBMP was also observed at pH >10 (Fig. S1c†). In this work, pH 7.4 Tris-HCl buffer solution was then selected to meet the requirements for physiological environment applications.

3.4. Fluorescence and absorption titrations

Under the optimal experimental conditions, fluorescence and absorption titrations were performed to evaluate the sensing performance. Fig. 6 shows the fluorescence spectra and titration curves with the continuous increase in the concentration of Cu^{2+} and Zn^{2+} in Tris-HCl buffer (10 mM, pH 7.4, 70% THF), respectively. It could be seen that the fluorescence intensity of the BBMP sensor at 542 nm gradually decreased with increasing the concentration of Cu^{2+}, and a good linear relationship was obtained (R^2 = 0.99027) within the concentration range 0–5 μM (Fig. 6a and b), with a detection limit of 0.16 μM (S/N = 3). As shown in Fig. 6c and d, upon the continuous addition of Zn^{2+}, the fluorescence intensity decreased at 541 nm and was enhanced at 465 nm, and a good linear relationship (R^2 = 0.99037) was obtained between the ratio of the fluorescence intensity (F_{465nm}/F_{541nm}) and the Zn^{2+} concentration within the concentration range 0–10 μM, with a detection limit of 0.1 μM (S/N = 3). When compared against the previously reported sensing systems, the present sensor showed a comparable and even better performance (Table S2†).

In addition, absorption titrations of Cu^{2+} and Zn^{2+} were also performed in Tris-HCl buffer (10 mM, pH 7.4, 70% THF), respectively. It was found that the absorption gradually decreased at 375 nm and increased at 420 nm with increasing the concentration of Cu^{2+} and Zn^{2+}, respectively (Fig. S2†). A well-defined isosbestic point was observed at 386 nm, suggesting a complex was formed between the BBMP sensor and metal ions.

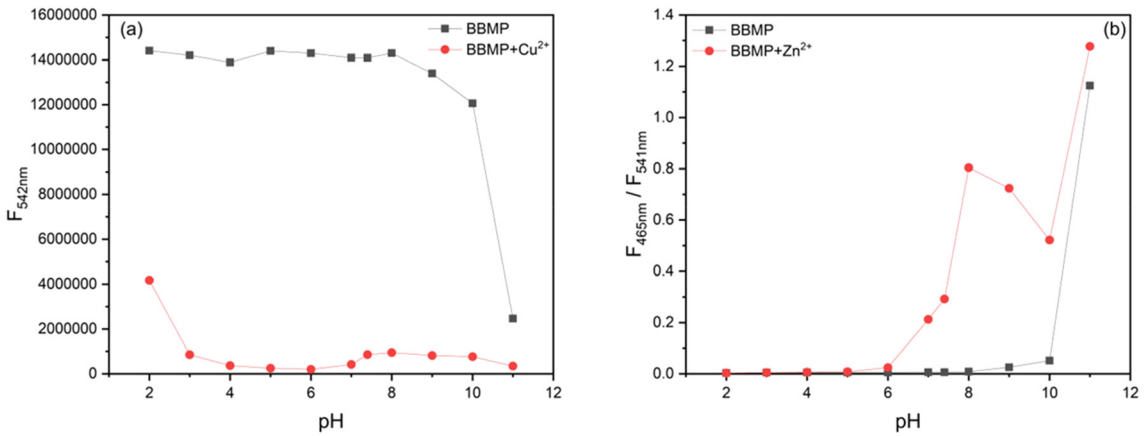

Fig. 5 Change in the fluorescence intensity of BBMP (10 μM) at different pH 2–11 upon the addition of 1 equiv. Cu^{2+} (a) and Zn^{2+} (b) in aqueous Tris-HCl solution (10 mM, pH 7.4, 70% THF), respectively. The excitation wavelength was 370 nm.

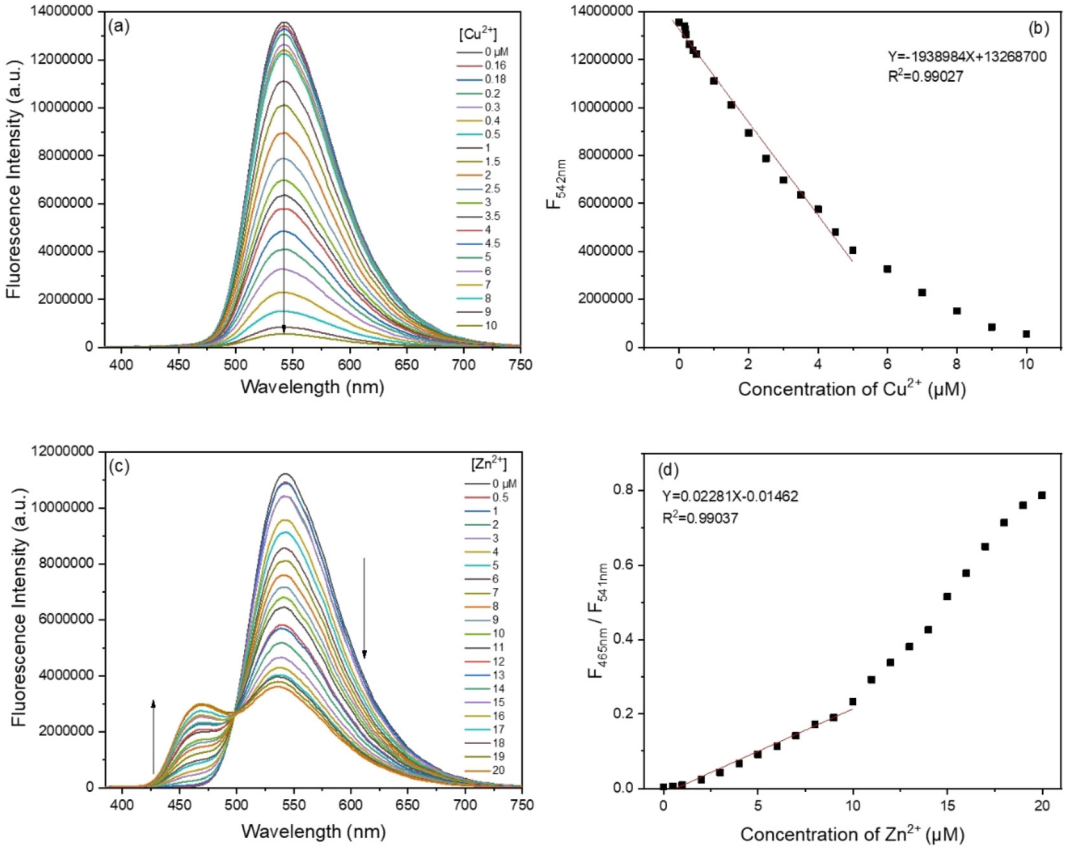

Fig. 6 Fluorescence titration spectra of BBMP (10 μM) upon the addition of different concentrations of Cu^{2+} (a) and Zn^{2+} (c) in aqueous Tris-HCl solution (10 mM, pH 7.4, 70% THF), as well as a corresponding linear correlation between the fluorescence intensity and concentrations of Cu^{2+} (b) and Zn^{2+} (d), respectively. The excitation wavelength was 370 nm.

3.5. Binding reversibility and modes of BBMP to Cu^{2+} and Zn^{2+}

Binding reversibility was investigated by the addition of ethylene diamine tetraacetic acid (EDTA) into the mixed solution of BBMP with Cu^{2+} or Zn^{2+}. It was observed that the introduction of EDTA could almost recover the fluorescence of BBMP at 542 nm, indicting the competitive chelation between EDTA and Cu^{2+} or Zn^{2+} would release the free BBMP and thus restore its fluorescence. The further addition of Cu^{2+} or Zn^{2+} could then cause fluorescence quenching again, confirming the binding between BBMP and Cu^{2+} or Zn^{2+} was reversible (Fig. S3†).

The coordination stoichiometric ratio between BBMP and Cu^{2+} or Zn^{2+} was investigated by the Job's plot method, with the absorption spectra and results shown in Fig. 7. Obviously,

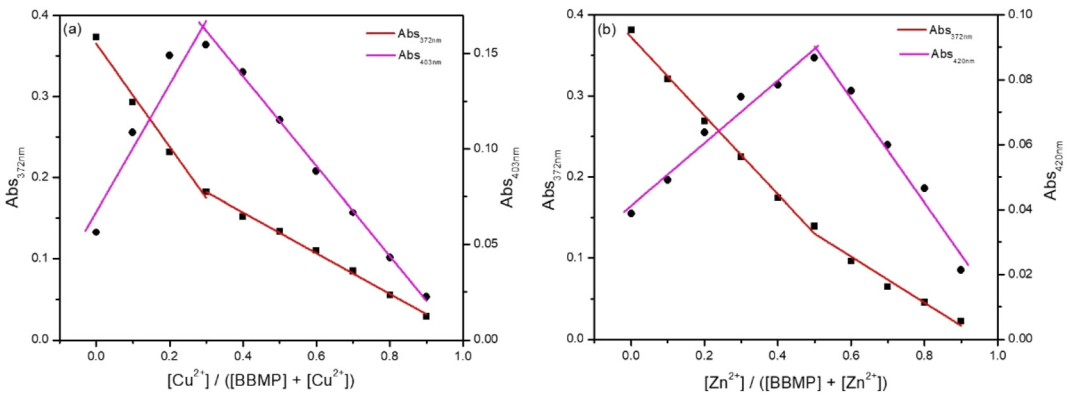

Fig. 7 Job plots for BBMP + Cu^{2+} (a) and BBMP + Zn^{2+} (b) complexes in aqueous Tris-HCl solution (10 mM, pH 7.4, 70% THF), respectively. Both the total concentrations of [BBMP] + [Cu^{2+}] = 20 μM and [BBMP] + [Zn^{2+}] = 20 μM.

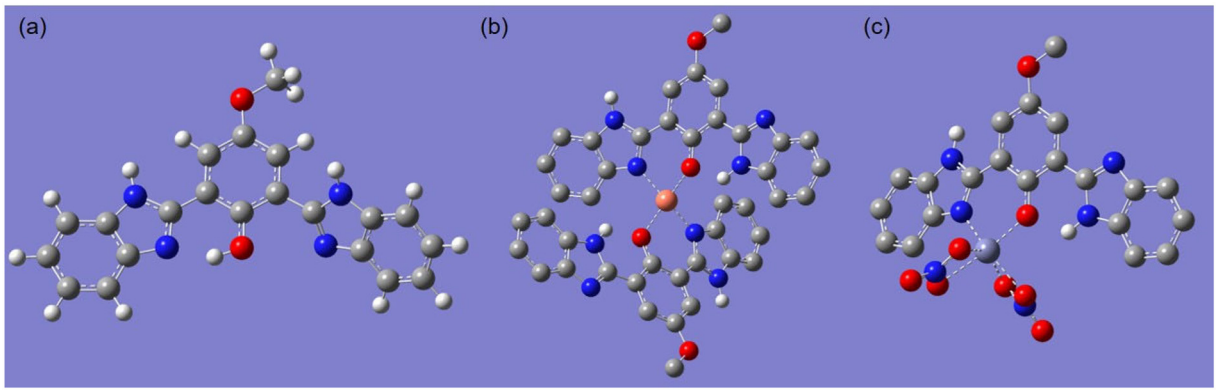

Fig. 8 Calculated molecular structures of BBMP (a) and its complexes with Cu^{2+} (b) and $Zn(NO_3)_2$ (c). Gray, blue, red, pink, light blue, and white colors denote C, N, O, Cu, Zn, and H atoms, respectively. All the H atoms except imine NH in (b) and (c) were omitted for clarity.

a 2 : 1 or 1 : 1 binding mode between BBMP and Cu^{2+} or Zn^{2+} was obtained. This was further confirmed by ESI-MS analysis of the mixture solution of BBMP with Cu^{2+} or Zn^{2+} in MeOH, respectively. A prominent peak was found at *m*/*z* 837.08774, which could be readily assigned to $[2BBMP–2H + Cu^{2+} + 2MeOH]^+$ species (Fig. S4a and c†). In addition, the mixture solution of BBMP with Zn^{2+} exhibited a complex peak at *m*/*z* 609.22409, which was attributed to $[BBMP + Zn(NO_3)_2 + 2MeOH]^+$ species (Fig. S4b and d†). This demonstrated that BBMP formed a 2 : 1 complex with Cu^{2+} and a 1 : 1 complex with Zn^{2+}. To further elucidate the binding mode, the ground-state molecular geometries of BBMP and its complexes with Cu^{2+} or $Zn(NO_3)_2$ were optimized by DFT calculations using the Gaussian 09 program package at the B3LYP/6-31 + G(d) level,[42] and the results are displayed in Fig. 8. The optimized BBMP showed that one benzimidazole unit was near coplanar with the phenol ring and the distance of the imidazole N···HO was 1.7199 Å, indicating the existence of intramolecular hydrogen-bonding that facilitated the ESIPT (Fig. 8a). However, the other benzimidazole unit in BBMP was found to be twisted about 53.8° from the phenol plane. Regarding the optimized complexes, both the imidazole N and phenolic O atoms were involved in coordination with metal ions, where the distances of O···Cu, N···Cu, O···Zn, and N···Zn were found to be 2.2186, 1.9812, 1.9968, and 2.0880 Å, respectively (Fig. 8b and c). Notably, the benzimidazole units involved in coordination were twisted 22.4° (Cu complex) or 16.2° (Zn complex) from the phenol plane. However, the non-coordinated benzimidazole units were almost planar with the phenol ring, where the distance of the phenolic O···HN (imine) was 1.8285 Å (Cu complex) or 1.9075 Å (Zn complex), suggesting intramolecular hydrogen-bonding was most probably involved in the complexes (Fig. 8b and c).

Therefore, the sensing mechanism could be understood by considering both the coordination interaction and natural property of the metal cation. Upon the addition of Cu^{2+}/Zn^{2+}, the complex formed between BBMP and the metal ion *via* the imidazole N atom and deprotonated phenolic group coordination could inhibit the ESIPT effect.[16] A turn-off response was observed in the presence Cu^{2+} due to its paramagnetic character, whereas a blue-shifted and turn-on fluorescence response with Zn^{2+} was observed, possibly resulting from a chelation-enhanced fluorescence effect.

3.6. Fluorescence detection of Cu^{2+} and Zn^{2+} in real samples

In order to investigate the practical application of the BBMP sensor, the fluorescence detection of Cu^{2+} and Zn^{2+} was performed in real water samples and zinc gluconate oral liquid, respectively. The lake water samples were collected from Songjiang Campus of Donghua University and filtrated to remove solid impurities before use. A standard addition method was used and five measurements were collected to estimate the relative standard deviation (RSD) and recovery rate. The analysis results are summarized in Tables 1 and 2. It was found that the recovery rate and RSD were 106–127.5% and 0.41–1.76% for Cu^{2+} detection in the real water samples (Table 1). The Zn^{2+} amount in zinc gluconate oral liquid was determined to be 4.12 μM, which matched well with the real value of 4 μM. The recovery rate and RSD were 99.5–108.14% and 1.19–6.02% for Zn^{2+} detection in the real samples

Table 1 Detection of Cu^{2+} in real water samples (*n* = 5)

Samples	Added Cu^{2+} (μM)	Detected Cu^{2+} (μM)	Recovery (%)	RSD (%)
Lake water	2	2.55 ± 0.09	127.50	1.76
	4	4.31 ± 0.05	107.75	0.41
Drinking water	2	2.48 ± 0.04	124.00	0.59
	4	4.24 ± 0.08	106.00	0.74

Table 2 Detection of Zn^{2+} in real samples (*n* = 5)

Samples	Added Zn^{2+} (μM)	Detected Zn^{2+} (μM)	Recovery (%)	RSD (%)
Lake water	4	4.65 ± 0.42	108.14	3.02
	7	7.60 ± 0.43	104.11	2.07
Zinc gluconate oral liquid	0	4.12 ± 0.41	—	3.90
	2	6.09 ± 0.21	99.50	1.19

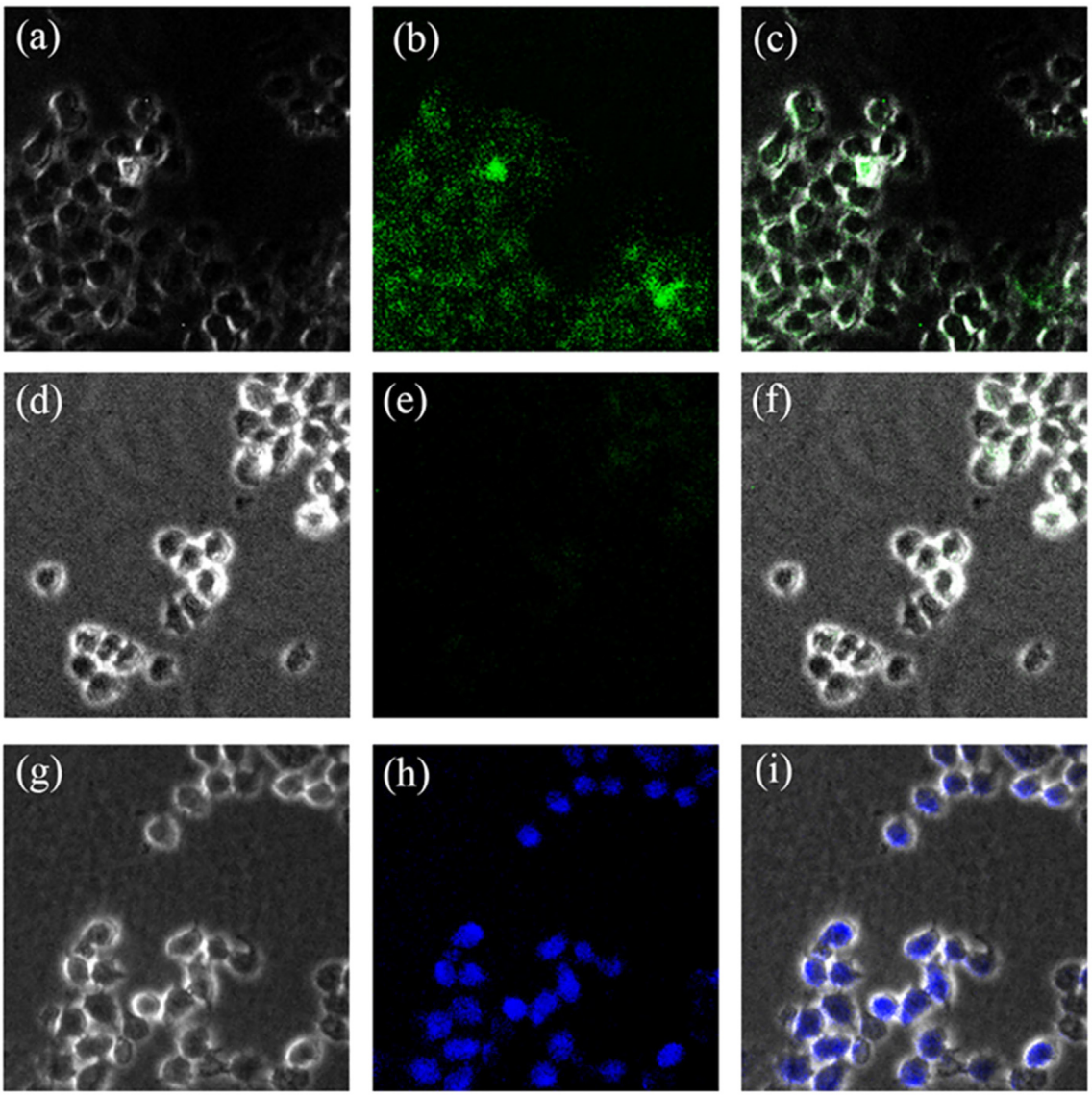

Fig. 9 Bright-field (a, d and g), dark-field (b, e and h), and merged (c, f and i) images of living HeLa cells. The HeLa cells were incubated with BBMP (10 μM) (a–c), BBMP and further with Cu^{2+} (20 μM) (d–f), and BBMP and further with Zn^{2+} (20 μM) (g–i) at 37 °C for 30 min, respectively.

(Table 2). Therefore, this demonstrated that the present BBMP sensor can be used as a promising fluorescent sensor for the rapid detection of Cu^{2+} and Zn^{2+} in practical water samples.

3.7. Fluorescence imaging in living cells

The application for Cu^{2+} and Zn^{2+} imaging in living cells was also investigated by confocal fluorescence microscopy. HeLa cells were first incubated with BBMP (10 μM) at 37 °C for 30 min, and subsequently incubated with 20 μM Cu^{2+} or Zn^{2+} and then observed under the confocal fluorescence microscope. Bright green fluorescence was observed in living cells incubated only with BBMP (Fig. 9a–c). Further incubation with Cu^{2+} caused a quenching of the green fluorescence (Fig. 9d–f), whereas a brilliant blue fluorescence was observed in living cells with further Zn^{2+} incubation (Fig. 9g–i). Thus the BBMP sensor is a promising sensor for Cu^{2+} and Zn^{2+} imaging in living cells.

4. Conclusions

We successfully developed a new benzimidazole-derived fluorescence chemosensor BBMP for Cu^{2+} and Zn^{2+} detection in aqueous solution. The BBMP exhibited an ESIPT fluorescence emission, which was quenched upon binding to Cu^{2+} and Zn^{2+} due to an inhibition of ESIPT. Notably, the BBMP also showed an 82 nm blue-shifted fluorescence from the original ESIPT emission upon binding Zn^{2+}, allowing the ratiometric detection. A Cu^{2+}-selective turn-off and Zn^{2+}-selective ratiometric turn-on fluorescent sensor was thus achieved. The binding mode

was studied with Job's plot, mass analysis, and DFT calculation, where a 2:1 or 1:1 complex was formed between BBMP and Cu^{2+} or Zn^{2+} with imidazole N and phenolic O atoms coordination. The linear range and detection limit were found to be 0–5 μM and 0.16 μM for Cu^{2+}, and 0–10 μM and 0.1 μM for and Zn^{2+}, respectively. Furthermore, the sensor was also successfully used for Cu^{2+} and Zn^{2+} detection in real water samples and fluorescence imaging in living cells.

Author contributions

Wan-Yu Zhu: investigation, data curation, and writing – original draft. Kai Liu: writing – review & editing. Xuan Zhang: conceptualization, methodology, writing – review & editing, supervision, funding acquisition.

Conflicts of interest

The authors declare that they have no known competing financial interests or personal relationships that could have appeared to influence the work reported in this paper.

Acknowledgements

This work was financially supported by the Research Foundation from National Innovation Center of Advanced Dyeing & Finishing Technology (No. 2022GCJJ10).

References

1 L. Li, J. Wang, S. Xu, C. Li and B. Dong, Recent progress in fluorescent probes for metal ion detection, *Front. Chem.*, 2022, **10**, 875241.
2 K. P. Carter, A. M. Young and A. E. Palmer, Fluorescent sensors for measuring metal ions in living systems, *Chem. Rev.*, 2014, **114**, 4564–4601.
3 M. H. Lee, J. S. Kim and J. L. Sessler, Small molecule-based ratiometric fluorescence probes for cations, anions, and biomolecules, *Chem. Soc. Rev.*, 2015, **44**, 4185–4191.
4 P. Piyanuch, S. Wangngae, A. Kamkaew, W. Wattanathana, S. Wannapaiboon, S. Impeng, W. Maneeprakorn, V. Promarak and K. Chansaenpak, Ultrasensitive fluorogenic chemosensor based on ESIPT phenomenon for selective determination of Cu^{2+} ion in aqueous system and its application in environmental samples and biological imaging, *Dyes Pigm.*, 2022, **205**, 110532.
5 M. Raju, R. R. Nair, I. H. Raval, S. Haldar and P. B. Chatterjee, A water soluble Cu^{2+}-specific colorimetric probe can also detect Zn^{2+} in live shrimp and aqueous environmental samples by fluorescence channel, *Sens. Actuators, B*, 2018, **260**, 364–370.
6 E. A. B. Pajarillo, E. Lee and D. K. Kang, Trace metals and animal health: Interplay of the gut microbiota with iron, manganese, zinc, and copper, Animal, *Nutrition*, 2021, **7**, 750–761.
7 A. Prabhu and M. Gadgil, Trace metals in cellular metabolism and their impact on recombinant protein production, *Process Biochem.*, 2021, **110**, 251–262.
8 B. Vellingiri, A. Suriyanarayanan, P. Selvaraj, K. S. Abraham, M. Y. Pasha, H. Winster, A. V. Gopalakrishnan, J. K. Reddy, N. Ayyadurai, N. Kumar, B. Giridharan, K. R. S. S. Rao, S. K. Nachimuthu, A. Narayanasamy, I. Mahalaxmi and D. Venkatesan, Role of heavy metals (copper (Cu), arsenic (As), cadmium (Cd), iron (Fe) and lithium (Li)) induced neurotoxicity, *Chemosphere*, 2022, **301**, 134625.
9 Y. Sun, W. Ding, J. Li, Y. Jia, G. Guo and Z. Deng, A novel and simple fluorescent chemical sensor SX based on AIE for relay recognition of Zn^{2+} and Cu^{2+} in aqueous system and analysis in logic gates, *J. Mol. Struct.*, 2022, **1252**, 132219.
10 B. Zha, S. Fang, H. Chen, H. Guo and F. Yang, An effective dual sensor for Cu^{2+} and Zn^{2+} with long-wavelength fluorescence in aqueous media based on biphenylacrylonitrile Schiff-base, *Spectrochim. Acta, Part A*, 2022, **269**, 120765.
11 J. C. Qin and Z. Y. Yang, Fluorescent chemosensor for detection of Zn^{2+} and Cu^{2+} and its application in molecular logic gate, *J. Photochem. Photobiol., A*, 2016, **324**, 152–158.
12 P. Ghorai, S. Banerjee, D. Nag, S. K. Mukhopadhyay and A. Saha, Design and synthesis of a novel fluorescent-colorimetric chemosensor for selective detection of Zn(II) and Cu(II) ions with applications in live cell imaging and molecular logic gate, *J. Lumin.*, 2019, **205**, 197–209.
13 Q. Niu, T. Sun, T. Li, Z. Guo and H. Pang, Highly sensitive and selective colorimetric / fluorescent probe with aggregation induced emission characteristics for multiple targets of copper, zinc and cyanide ions sensing and its practical application in water and food samples, *Sens. Actuators, B*, 2018, **266**, 730–743.
14 H. Thomas, J. Naimhwaka, P. Endjala and V. Uahengo, ESIPT-influenced C3-symmetry, disk-shaped fluorescence turn-on probe for Zn^{2+} based on melamine-naphthyl moiety with high affinity towards Cu^{2+} in CH_3CN, *Results in Optics*, 2022, **6**, 100215.
15 H. Fang, P. C. Huang and F. Y. Wu, A highly sensitive fluorescent probe with different responses to Cu^{2+} and Zn^{2+}, *Spectrochim. Acta, Part A*, 2019, **214**, 233–238.
16 J. S. Ganesan, S. Gandhi, K. Radhakrishnan, A. Balasubramaniem, M. Sepperumal and S. Ayyanar, Execution of julolidine based derivative as bifunctional chemosensor for Zn^{2+} and Cu^{2+} ions: Applications in bio-imaging and molecular logic gate, *Spectrochim. Acta, Part A*, 2019, **219**, 33–43.
17 A. Jayaraj, M. S. Gayathri, G. Sivaraman and C. A. Swamy P, A highly potential acyclic Schiff base fluorescent turn on sensor for Zn^{2+} ions and colorimetric chemosensor for Zn^{2+}, Cu^{2+} and Co^{2+} ions and its applicability in live cell imaging, *J. Photochem. Photobiol., B*, 2022, **226**, 112371.
18 S. M. Hwang and C. Kim, Fluorescent detection of Zn^{2+} and Cu^{2+} by a phenanthrene-based multifunctional chemosensor that acts as a basic pH indicator, *Inorg. Chim. Acta*, 2018, **482**, 375–383.

19 R. Arabahmadi, Antipyrine-based Schiff base as fluorogenic chemosensor for recognition of Zn^{2+}, Cu^{2+} and $H_2PO_4^-$ in aqueous media by comparator, half subtractor and integrated logic circuits, *J. Photochem. Photobiol., A*, 2022, **426**, 113762.

20 M. S. Kim, T. G. Jo, M. Yang, J. Han, M. H. Lim and C. Kim, A fluorescent and colorimetric Schiff base chemosensor for the detection of Zn^{2+} and Cu^{2+}: Application in live cell imaging and colorimetric test kit, *Spectrochim. Acta, Part A*, 2019, **211**, 34–43.

21 V. Kumar, U. Diwan, N. Tyagi, R. K. Mishra, M. K. Singh and K. K. Upadhyay, A coumarin based fluorescent probe enabling nanomolar detection of Zn^{2+} and Cu^{2+}, *J. Photochem. Photobiol., A*, 2022, **425**, 113692.

22 X. He, Q. Xie, J. Fan, C. Xu, W. Xu, Y. Li, F. Ding, H. Deng, H. Chen and J. Shen, Dual-functional chemosensor with colorimetric / ratiometric response to Cu(II) / Zn(II) ions and its applications in bioimaging and molecular logic gates, *Dyes Pigm.*, 2020, **177**, 108255.

23 J. C. Qin and Z. Y. Yang, Design of a novel coumarin-based multifunctional fluorescent probe for $Zn^{2+}/Cu^{2+}/S^{2-}$ in aqueous solution, *Mater. Sci. Eng., C*, 2015, **57**, 265–271.

24 C. Liu, J. C. Qin, J. Xue, L. M. Tian, T. R. Li and Z. Y. Yang, Development of a novel fluorescent probe for $Zn^{2+}/Cu^{2+}/S^{2-}$ in different solutions based on benzocoumarin derivative, *J. Photochem. Photobiol., A*, 2019, **385**, 112091.

25 Y. Wang, P. D. Mao, W. N. Wu, X. J. Mao, Y. C. Fan, X. L. Zhao, Z. Q. Xu and Z. H. Xu, New pyrrole-based single-molecule multianalyte sensor for Cu^{2+}, Zn^{2+}, and Hg^{2+} and its AIE activity, *Sens. Actuators, B*, 2018, **255**, 3085–3092.

26 T. S. Aysha, M. B. I. Mohamed, M. S. El-Sedik and Y. A. Youssef, Multi-functional colorimetric chemosensor for naked eye recognition of Cu^{2+}, Zn^{2+} and Co^{2+} using new hybrid azo-pyrazole / pyrrolinone ester hydrazone dye, *Dyes Pigm.*, 2021, **196**, 109795.

27 C. M. Pang, S. H. Luo, K. Jiang, B. W. Wang, S. H. Chen, N. Wang and Z. Y. Wang, A dual-channel sensor containing multiple nitrogen heterocycles for the selective detection of Cu^{2+}, Hg^{2+} and Zn^{2+} in same solvent system by different mechanism, *Dyes Pigm.*, 2019, **170**, 107651.

28 X. Pei, Y. Pan, L. Zhang and Y. Lv, Recent advances in ratiometric luminescence sensors, *Appl. Spectrosc. Rev.*, 2021, **56**, 324–345.

29 S.-H. Park, N. Kwon, J.-H. Lee, J. Yoon and I. Shin, Synthetic ratiometric fluorescent probes for detection of ions, *Chem. Soc. Rev.*, 2020, **49**, 143–179.

30 P. S. Kumar and K. P. Elango, A simple organic probe for ratiometric fluorescent detection of Zn(II), Cd(II) and Hg(II) ions in aqueous solution via varying emission colours to distinguish one another, *Spectrochim. Acta, Part A*, 2020, **241**, 118610.

31 F. A. S. Chipem, S. K. Behera and G. Krishnamoorthy, Ratiometric fluorescence sensing ability of 2-(2′-hydroxyphenyl)benzimidazole and its nitrogen substituted analogues towards metal ions, *Sens. Actuators, B*, 2014, **191**, 727–733.

32 Y. Wu, J. You, L. Guan, J. Shi, L. Cao and Z. Wang, Progress in the synthesis and application of benzimidazole-based fluorescent chemosensors, *Chin. J. Org. Chem.*, 2015, **35**, 2465–2486.

33 M. Qin, D. Jin, W. Che, Y. Jiang, L. Zhang, D. Zhu and Z. Su, Fluorescence response and detection of Cu^{2+} with 2-(2-hydroxyphenyl)benzimidazole in aqueous medium, *Inorg. Chem. Commun.*, 2017, **75**, 25–28.

34 L. Wang, X.-Y. Zheng, X. Zhang and Z.-J. Zhu, A quinoline-based fluorescent chemosensor for palladium ion (Pd^{2+})-selective detection in aqueous solution, *Spectrochim. Acta, Part A*, 2021, **249**, 119283.

35 L. Wang, W.-Y. Zhu and X. Zhang, Selective and sensitive fluorescence detection of Pd (II) in 100% water and imaging application in living cells, *Chin. J. Anal. Chem.*, 2022, **50**, 100155.

36 S. Anbu, A. Paul, K. Surendranath, N. S. Solaiman and A. J. L. Pombeiro, A benzimidazole-based new fluorogenic differential/sequential chemosensor for Cu^{2+}, Zn^{2+}, CN^-, $P_2O_7^{4-}$, DNA, its live-cell imaging and pyrosequencing applications, *Sens. Actuators, B*, 2021, **337**, 129785.

37 X. Zhang, J.-Y. Liu, W.-W. Ma and M.-L. Yang, Near-infrared fluorescence of π-conjugation extended benzothiazole and its application for biothiol imaging in living cells, *J. Mater. Chem. B*, 2016, **4**, 6662–6669.

38 Y. Zhou, L. Zhang, X. Zhang and Z.-J. Zhu, Development of a near-infrared ratiometric fluorescent probe for glutathione using an intramolecular charge transfer signaling mechanism and its bioimaging application in living cells, *J. Mater. Chem. B*, 2019, **7**, 809–814.

39 X. Zhang, L. Zhang, W.-W. Ma, Y. Zhou, Z.-N. Lu and S. Xu, A near-infrared ratiometric fluorescent probe for highly selective recognition and bioimaging of cysteine, *Front. Chem.*, 2019, **7**, 32.

40 K. Takagi, Y. Yamada, R. Fukuda, M. Ehara and D. Takeuchi, ESIPT emission behavior of methoxy-substituted 2-hydroxyphenylbenzimidazole isomers, *New J. Chem.*, 2018, **42**, 5923–5928.

41 X. Zhang and J.-Y. Liu, Solvent dependent photophysical properties and near-infrared solid-state excited state intramolecular proton transfer (ESIPT) fluorescence of 2,4,6-tris- benzothiazolylphenol, *Dyes Pigm.*, 2016, **125**, 80–88.

42 M. J. Frisch, G. W. Trucks, H. B. Schlegel, G. E. Scuseria, M. A. Robb, J. R. Cheeseman, G. Scalmani, V. Barone, B. Mennucci, G. A. Petersson, H. Nakatsuji, M. Caricato, X. Li, H. P. Hratchian, A. F. Izmaylov, J. Bloino, G. Zheng, J. L. Sonnenberg, M. Hada, M. Ehara, K. Toyota, R. Fukuda, J. Hasegawa, M. Ishida, T. Nakajima, Y. Honda, O. Kitao, H. Nakai, T. Vreven, J. A. Montgomery Jr., J. E. Peralta, F. Ogliaro, M. Bearpark, J. J. Heyd, E. Brothers, K. N. Kudin, V. N. Staroverov, T. Keith, R. Kobayashi, J. Normand, K. Raghavachari, A. Rendell, J. C. Burant, S. S. Iyengar, J. Tomasi, M. Cossi, N. Rega, J. M. Millam, M. Klene, J. E. Knox, J. B. Cross, V. Bakken, C. Adamo, J. Jaramillo, R.

Gomperts, R. E. Stratmann, O. Yazyev, A. J. Austin, R. Cammi, C. Pomelli, J. W. Ochterski, R. L. Martin, K. Morokuma, V. G. Zakrzewski, G. A. Voth, P. Salvador, J. J. Dannenberg, S. Dapprich, A. D. Daniels, O. Farkas, J. B. Foresman, J. V. Ortiz, J. Cioslowski and D. J. Fox, *Gaussian 09, Revision C.01*, Gaussian, Inc., Wallingford CT, 2010.